Lab on a Chip

RSC Publishing

PAPER

View Article Online
View Journal | View Issue

High throughput and high yield nanofabrication of precisely designed gold nanohole arrays for fluorescence enhanced detection of biomarkers

Cite this: *Lab Chip*, 2013, **13**, 2405

Ten It Wong,[a] Shan Han,[b] Lin Wu,[c] Yi Wang,[d] Jie Deng,[a] Christina Yuan Ling Tan,[a] Ping Bai,[c] Yee Chong Loke,[a] Xin Da Yang,[b] Man Siu Tse,[b] Sum Huan Ng[e] and Xiaodong Zhou*[a]

Received 20th December 2012,
Accepted 26th March 2013

DOI: 10.1039/c3lc41396a

www.rsc.org/loc

Fluorescence excitation enhancement by plasmonic nanostructures such as gold nanohole arrays has been a hot topic in biosensing and bioimaging in recent years. However, the high throughput and high yield fabrication of precisely designed metal nanostructures for optimized fluorescence excitation remains a challenge. Our work is the first report combining nanopattern nickel mould fabrication and UV imprinting for gold nanostructure mass fabrication in high yield. We report our successful gold nanohole array mass fabrication on a 4'' glass wafer, by first fabricating a high fidelity nickel mould, then using the mould for UV nanoimprinting on a polymer coated on the glass, evaporating the gold film on the glass wafer, and lifting off the polymer to obtain a gold nanohole array on the glass. Our optimized process for wafer fabrication can achieve almost 100% yield from nanoimprinting to gold lift-off, while the fabricated nickel mould has >70% defect-free area with the rest having a few scattered defects. In our work, the size and pitch of the gold nanohole array are designed to enhance the fluorescent dye Alexa 647. When the fabricated gold nanohole array is used for prostate specific antigen (PSA) detection by establishing a sandwiched fluorescence assay on the gold surface, a detection limit of 100 pg ml^{-1} is achieved, while with a same thickness of gold film, only 1 ng ml^{-1} is detected.

Introduction

Plasmonic resonance of metal nanostructures redistributes the electromagnetic field energy, by absorbing the light intensity at a certain wavelength and focusing the power at the corner of the metal nanostructures like antenna. Researchers have been investigating the application of gold films[1–4] and metal nanohole(s)[5–12] or particles[13–16] for fluorescence excitation enhanced biosensing or imaging for decades. More attention has been paid to metal nanostructure based fluorescent dye excitation, because although gold films can also be used to generate surface plasmon resonance (SPR) for dye excitation, this requires complicated optical momentum matching apparatus for SPR generation. In comparison, metal nanostructures can generate localized surface plasmon resonance (LSPR) for dye excitation by light illumination at any angle, thus they are ideal for the configuration of a portable detection system with growing demands.

In previous studies using fluorescence to enhance dyes using gold nanoholes,[5–12] most were conducted by coating a layer of fluorescent dye on the surface to investigate the enhancement effects of the plasmonic field, without carrying out any biomarker detection. These gold nanostructures were precisely fabricated by e-beam lithography or milled by a focused ion beam, which is expensive and time consuming. Tabakman *et al.* demonstrated that the biomarkers could be detected at a high sensitivity by plasmonic fluorescence enhancement,[13] however, the gold nanostructures were randomly distributed islands with broad transmission spectra, and the right gold nanoparticle dimensions and thickness could be found only by trial and error.

It is known that to obtain the brightest fluorescence signal, the LSPR scattering peak should be about 40–120 meV higher in energy than a dye's emission peak, and the plasmonic spectral shape should coincide with the dye's excitation spectrum.[16] Metal nanohole arrays have a well controlled

[a]*Institute of Materials Research and Engineering, A*STAR (Agency for Science, Technology and Research), 3 Research Link, 117602, Singapore. E-mail: donna-zhou@imre.a-star.eud.sg; Fax: +65 6872 7522; Tel: +65 6872 7522*
[b]*School of Electrical and Electronic Engineering, Nanyang Technological University, 50 Nanyang Avenue, 639798, Singapore*
[c]*Electronics and Photonics Department, Institute of High Performance Computing, A*STAR (Agency for Science, Technology and Research), 1 Fusionopolis Way, 138632, Singapore*
[d]*Centre for Biomimetic Sensor Science, Nanyang Technological University, 50 Nanyang Drive, Research Techno Plaza 6th Storey, XFrontiers Block, 637553, Singapore*
[e]*Singapore Institute of Manufacturing Technology, A*STAR (Agency for Science, Technology and Research), 71 Nanyang Drive, 638075, Singapore*

plasmonic peak and narrower band to fulfil these conditions. However, it is challenging to fabricate metal nanohole arrays with low cost and high yield. Although colloidal lithography has been utilized for LSPR sensing[17–20] and it is possible to use it to fabricate periodic gold nanohole arrays by closely-packing the colloids and shrinking the size of the colloids by annealing,[21,22] it is very difficult to fabricate defect free gold nanohole arrays in an area where its critical size is larger than 100 μm. Stencil lithography,[23] where the evaporated metal atoms pass through a stencil and deposit on the substrate to form nanopatterns, is also an inexpensive method to mass fabricate metal nanostructures on a substrate, but due to the gap between the stencil and the substrate, the metal patterns suffer from a blurring effect and the patterns do not have sharp corners. Compared with the literature, the contributions of this paper lie in (1) the fabrication of a designed gold nanohole array on a glass wafer with high quality and high yield in a mass fabrication route; and (2) the proof-of-concept experiment of using the fabricated gold nanohole array to detect prostate specific antigen (PSA), a biomarker indicating male prostate cancer.

To fabricate the designed gold nanohole array onto a glass chip cost-effectively, our strategy is to fabricate a 4″ nickel mould, and use the mould for UV imprinting to fabricate the gold nanohole array at wafer level. Nickel moulds are very durable, and have been reported to be used ten thousand times without wearing,[24] and our method of fabricating a nickel mould is highly cost-effective by directly electroplating on the e-beam written nanopatterns on a silicon wafer. There are several reports on fabricating nickel moulds with microstructures by electroplating on a photoresist patterned silicon wafer.[25–33] However, they are all in microsize, and nanosized moulds need more stringent quality control and process optimization. To the best of our knowledge, we are the first to fabricate a nanosized nickel mould in this way. Our fabricated nickel mould has high fidelity compared with a deep reactive ion etching (DRIE) etched silicon mould or a silicon mould duplicated polymer mould, because silicon etching degrades the shapes of nanopattern. With our method, the aspect ratio of the mould can be very high, because the aspect ratio of the resist pattern written by e-beam can be fully transferred into the nickel mould.

UV nanoimprinting is a popular tool used in fabricating metal nanostructures for plasmonics.[34–38] Compared with thermal nanoimprinting,[39–42] it imprints at low pressure and low temperature, consumes less energy and takes less time, reduces the breakage of the substrate glass wafer, and demonstrates good tolerance to accidental dust/particles between the mould and the glass substrate. Attributed to our high quality nickel mould and UV nanoimprinting, which enables the polymer to fill the corners of the high density nanostructures well, the yield of our gold nanohole array fabricated on a glass wafer is close to 100% from nanoimprinting to gold lift-off, while the nickel mould has >70% totally defect-free area.

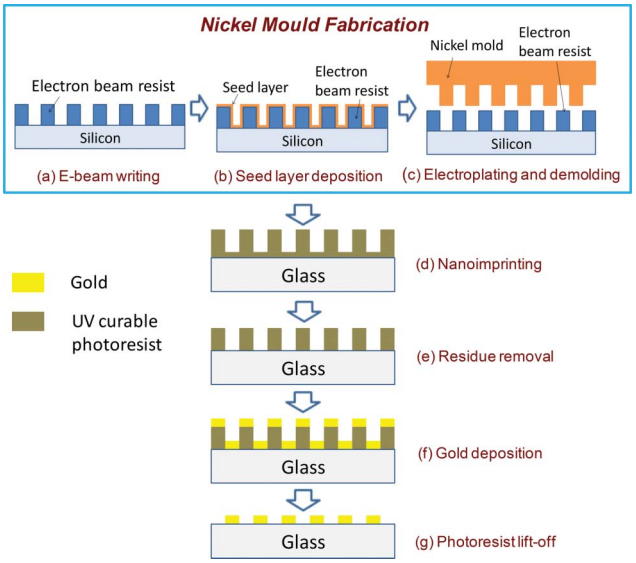

Fig. 1 Our method of mass fabricating metal nanostructures on glass wafers. (a)–(c) show nickel mould fabrication, and (d)–(f) show the fabrication of the pure gold nanohole array on glass.

The glass wafer with fabricated gold nanohole array was diced and used for a fluorescence enhancement experiment using total internal reflection (TIR) fluorescence spectroscopy in the TE mode. Our PSA detection was conducted with a sandwich assay (capture antibody)–PSA–(detection antibody with fluorescent dye) built on the 50 nm thick gold nanohole array on glass, which shows a limit of detection (LOD) of 100 pg ml^{-1}. The same assay built on a 50 nm thick gold film as a control demonstrates a LOD of 1000 pg ml^{-1}.

Overall, we have for the first time achieved high yield and high fidelity gold nanostructure mass fabrication, and have applied the fabricated gold nanohole array for fluorescence enhancement for biomarker detection. Since a portable detector for fluorescence detection is easy to fabricate, the chip and bioassay established in this work can be readily incorporated into a point-of-care system for medical diagnostics.

Experiments

The overall fabrication process is illustrated in Fig. 1.

The high fidelity nickel mould in our study was fabricated with the approach of (a) using e-beam lithography to write a pattern on the resist coated on a substrate such as silicon, (b) coating a metal seed layer on the nanopattern, and (c) electroplating the nickel mould and separating the mould and the substrate by resolving the resist in solvent.

When a durable nanoimprinting mould is available, our mass fabrication of the gold structures at wafer level was realized with the steps of (d) coating the polymer on the substrate, and UV nanoimprinting the nanopattern of the mould onto the polymer, (e) etching the polymer layer to

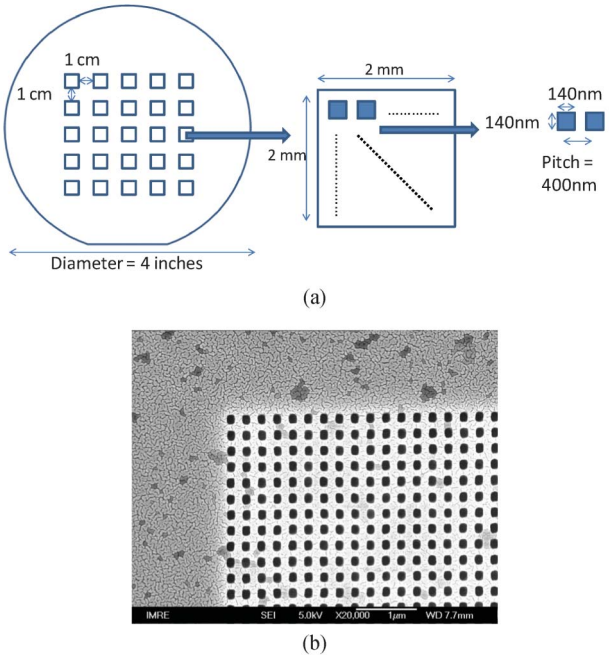

Fig. 2 (a) Arrangement of 25 2 mm × 2 mm areas of square nanoholes on a 4′′ wafer. (b) Field emission scanning electron microscope (FESEM) image of an exemplified nanohole array (square length is 120 nm, pitch is 240 nm) written by e-beam at the corner of a patterned area.

expose the substrate at the indented areas of the polymer, (f) evaporating a metal thin film onto the substrate, and (g) lifting off the polymer to obtain the metal nanostructure on the substrate.

Nickel mould fabrication

The gold nanopatterns designed for fluorescence enhancement of the dye Alexa647[43] are 140 nm × 140 nm square nanoholes forming an array at a pitch of p = 400 nm, based on our previous simulations.[44,45]

For mass fabrication, 25 2 mm × 2 mm areas of the designed patterns were written on a layer of electron beam resist, 220 nm thick of NEB22, coated on a 600 μm thick 4′′ silicon wafer, by using ELS-7000 (Elionix) to write with an exposure of 178 μC cm^{-2} at a current of 800 pA. Oxylene was used to develop the resist. The arrangement of the nanopatterns on the wafers and representative nanopatterns written by e-beam are presented in Fig. 2.

Since silicon wafers with patterned photoresists are not conductive enough, a metal seed layer such as copper, nickel or aluminium was coated on the silicon wafer, for the wafer to be electroplated in a Technotrans AG, RD.50 plating system in a nickel sulfamate bath. Two-step electroplating was carried out. The initial stage was for 95 min at a lower current density of 0.7 A dm^{-2} for a complete filling of the nickel into the nanopatterns. After 12 μm of nickel was electroplated, the current density was increased to 12 A dm^{-2} for the second accelerated stage for 125 min to reach a final nickel mould thickness of 300 μm.

The nickel mould was separated from the silicon substrate by soaking overnight in Microposit Remover 1165 purchased from Rohm and Haas Electronic Materials LLC, to remove the e-beam resist. The silicon substrate was cleaned for reuse with Microposit Remover 1165. Then, the nickel mould was dehydrated in an oven at 100 °C for 3 h and cleaned in a Trion Plasma Etching System with O_2 gas for 3 min.

Gold nanostructure fabrication

The fabricated nickel mould was used for nanoimprinting on a 4′′ glass wafer coated with 300 nm thick UV curable mr-UVCur21-300 nm photoresist, purchased from micro resist technology GmbH. (Heptadecafluoro-1,1,2,2-tetrahydrodecyl)-trichlorosilane (FDTS) was coated on the nickel mould in an AVC-150 M (Sorona Inc.) machine at a temperature of 80 °C, so as to form an anti-adhesive layer for demoulding the mould from the photoresist after nanoimprinting.

The nanopatterns on the nickel mould were nanoimprinted on mr-UVCur21-300 nm with an Obducat Imprinter at a pressure of 10 bar and a temperature of 40 °C for 10 min. Then the mould, the photoresist and the glass wafer were transferred into a DYMAX Light Curing System (Model 2000 Flood) to photocure for 30 s. After nanoimprinting, the nickel mould could be easily demoulded from the glass wafer.

To fabricate the gold nanohole array on glass, the nickel mould was with nanohole patterns. After nanoimprinting, the photoresist on the glass substrate was blank etched in an Oxford reactive ion etching (RIE) system with an O_2 gas flow of 10 sccm at 50 W for 2 s, to expose the glass on the indented areas. The photoresist thickness to be etched should be as small as possible, as it is common to employ a photoresist thickness 3 times the metal thickness for a successful lift-off process. Then a thin chromium (Cr) layer for metal adhesion and a gold (Au) layer for plasmonics were deposited onto the glass wafer in a Denton Explorer E-beam deposition machine. The deposition rate for chromium was 1 Å s^{-1}, and for gold was 2 Å s^{-1}. UV curable photoresist is more difficult to lift-off than the thermal nanoimprint photoresist, thus the lift-off was carried out by Trion O_2 plasma etching for 3 min followed by sonification of samples in acetone for 15 s.

For the convenience of scanning electron microscope (SEM) and atomic force microscope (AFM) inspections, the gold nanohole arrays fabricated on the glass wafers were diced into 5 mm × 5 mm chips, with gold nanoholes occupying the central 2 mm × 2 mm of the chip.

Optical spectra measurement of gold nanohole arrays

The gold nanohole array spectra were measured with a Shimadzu UV-2450 spectrometer. Because the gold nanohole array occupies an area of only 2 mm × 2 mm on the 5 mm × 5 mm LSPR chip, while the interrogative beam size is around 5 mm in diameter, the spectral measurements were conducted by sticking the gold nanohole chip onto a 2 mm thick PMMA sheet with a 2 mm × 2 mm opening.

As illustrated in Fig. 3, a reference spectrum was taken by covering the backside of a PMMA sheet with opaque plastic tape. Then the gold nanohole array spectrum in air was taken, when an LSPR chip was adhered to the transparent side of the PMMA sheet, with gold facing the opening. To measure the

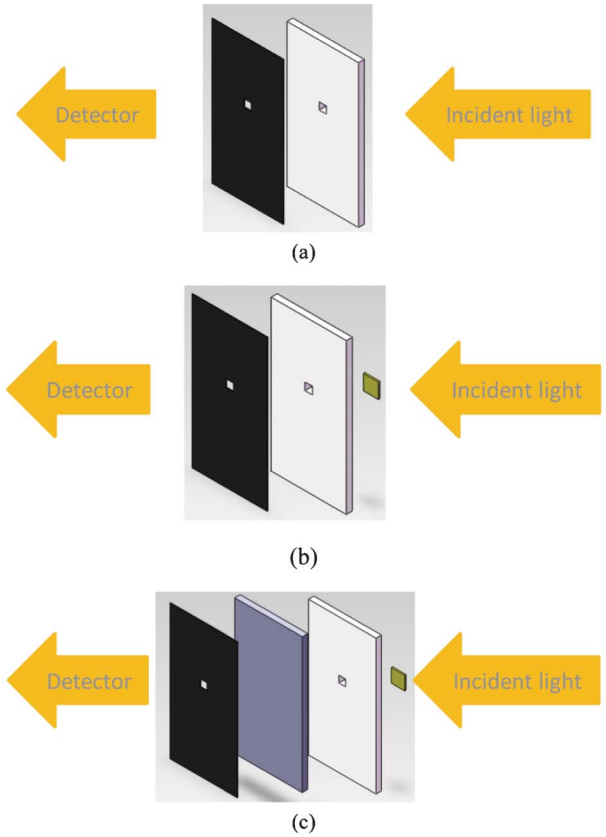

Fig. 3 Steps for measuring gold nanohole array spectra in air and water. (a) The reference spectrum is taken by stacking a 2 mm thick PMMA sheet (white, with an opening of 2 mm × 2 mm) with an opaque plastic tape having the same opening. (b) To take the spectra in air, the 5 mm × 5 mm LSPR chips were aligned and stuck to the PMMA sheets. (c) To take the spectra in water, a 2 mm thick glass slide was used to trap the water in the opening of the PMMA sheet.

spectra of the LSPR chips in water, a laminate stacking of (1) opaque plastic tape with an opening, (2) a 2 mm thick glass slide, (3) PMMA with an opening, and (4) the chip with gold facing the opening was formed, by trapping water in the PMMA opening between the glass slide and the chip.

Fluorescence enhancement experiment

In the experiment, prostate specific antigen (PSA), capture antibody (c-Ab) and detection antibody (d-Ab) were purchased from SunnyLab of SCIPAC Ltd. Thiol-COOH, EDC and NHS were purchased from Sigma-Aldrich.

The Molecular Probes Alexa Fluor® 647 Protein Labeling Kit was purchased from Invitrogen. The procedure of labeling the PSA d-Ab was based on the manual of the kit.[43] On recording the UV-vis spectrum of the labeled d-Ab, two peaks were found, one at 280 nm with A280 = 0.07929 attributed to the d-Ab, the other at 650 nm with A650 = 0.52849 attributed to the fluorescent dye. Thus the d-Ab concentration after labeling was calculated[43] to be 6.25 μM, and each d-Ab is labeled with 7 Alexa647 dye molecules.

The LSPR substrate used in the PSA experiments is a gold nanohole array on glass with p = 400 nm, size = 140 nm × 140 nm, and T = 50 nm. For the convenience of the experiments, the gold nanohole array area of 2 mm × 2 mm was fabricated on a 2 cm × 2 cm substrate. A 50 nm thick gold film was coated on a glass chip for control experiments.

To immobilize the c-Ab on the gold surface, the substrate was modified with thiol-COOH by incubating in a 1 mM thiol-COOH ethanol solution overnight. Afterwards, the substrate was rinsed with ethanol and dried with nitrogen. The substrate was fixed in a flow-cell with volume around 100 μl and circulated in buffer solution with a parasitic pump, and the carbon acid groups on the substrate were activated with freshly prepared EDC (37.5 mg ml^{-1}) and NHC (11.5 mg ml^{-1}) water solution. The capturing antibodies were immobilized on the surface by 2 h incubation of the substrate in 50 μg ml^{-1} c-Ab buffer solution.

PSA was detected through a (c-Ab)–antigen–(d-Ab) sandwich immunoassay. Phosphate-buffered saline with Tween-20 (PBST) buffer spiked with different concentrations of PSA was incubated on the substrate with a flow-cell for 30 min. After 2 min rinsing with PBST buffer, 10 nM detection antibodies labeled with Alexa647 were pumped into the flow-cell and incubated for 20 min. The fluorescence was measured with a home-made total internal reflection (TIR) fluorescence spectroscope under the TE mode.[1,2] In the TIR fluorescence system, light at the wavelength of 633 nm was shed from the bottom of a prism at a total reflection angle of 71°, *i.e.*, the angle between the normal of the glass surface and the light beam is 71°. Under the TE mode, no surface plasmon resonance will be generated on the gold film or the gold nanohole array. The LSPR on the gold nanohole array is polarization independent, thus the dye excitations are enhanced by the LSPR.

Results and discussion

Nanostructure characterization

In order to reach a high fabrication yield of the gold nanohole array on the whole wafer, the nanofabricated patterns in each step must be of high quality. Since nickel has magnetism, the nickel mould tends to be sucked by the electron objective column and cannot be viewed by SEM. After cleaning, the nanopatterns on the nickel mould were inspected under an optical microscope. Fig. 4(a) shows a corner of a nickel mould with 2 mm × 2 mm area filled with nanoholes at a size of 140 nm × 140 nm, a pitch of 400 nm, and a depth of 220 nm. Different areas of the nickel mould were inspected, the rest of the nanopatterns on the 4″ mould are of similar quality to those shown in Fig. 4(a).

The quality of the mould was further indirectly verified by imprinted patterns under SEM and AFM. The SEM and AFM images were inspected after dicing the glass wafer.

Fig. 4(b) shows an SEM image of the imprinted photoresist nanopillars (using the mould shown in Fig. 4(a)) after 75 nm of gold are deposited, and a gold nanohole array obtained on a glass wafer after lift-off is presented in Fig. 4(c). Fig. 4(c) shows that the AFM image over a 10 μm × 10 μm area on a glass substrate contains 625 nanoholes. Some spots are stained in Fig. 4(c). However, none of them are at the location of a

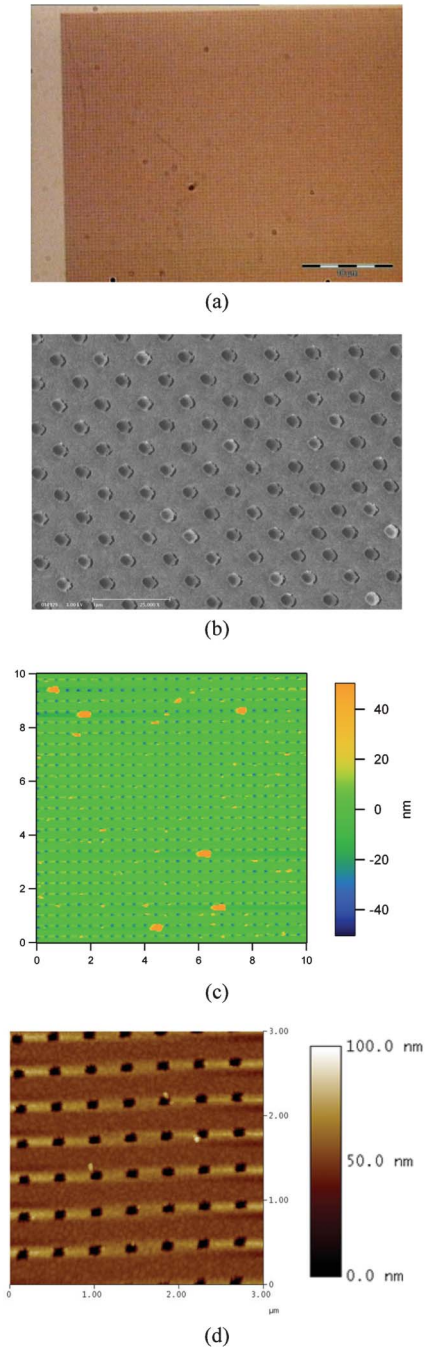

Fig. 4 (a) Image of a 4′′ nickel mould with 220 nm depth nanoholes under an optical microscope, at the corner of a 2 mm × 2 mm patterned square. (b) 20° tilted SEM image of the photoresist on glass, after being nanoimprinted by the mould in (a) and 75 nm of gold deposited. (c) AFM image of (b) after lift-off, where the patterns form a 75 nm thick gold nanohole array on glass. (d) AFM image of a 50 nm thick gold nanohole array on glass. All nanopatterns are with p = 400 nm and size of 140 nm × 140 nm.

nanohole on the array. Based on our fabrication process, they should not be caused by defects on the nickel mould or the photoresist after nanoimprinting, because the adjacent nanohole patterns are not affected at all; they also cannot be irregular gold grains, because the size is too large (some are ⩾400 nm) and the absorption spectral measurement in Fig. 5 is not affected. We attribute the spots on the AFM image to dust on the chip. Fig. 4(d) shows a 50 nm thick gold nanohole array fabricated on glass, and the gold nanoholes inspected in different areas are highly similar.

For the patterns in Fig. 4(b)–(d) obtained from different diced chips, high repeatability and reproducibility from wafer to wafer and batch to batch were found. We have fabricated about 30 wafers, did not see any wear of the mould, and hundreds of chips were measured under SEM and AFM by different research groups, without any deviations observed. This reveals that the qualities of our fabricated chips are high in terms of the reliability, uniformity, and robustness.

We also noticed that the mould fabrication is the key. With a good mould, the yield from nanoimprinting to gold lift-off is close to 100%. It is difficult to fabricate a nickel mould without any defect, but we can easily achieve >70% defect-free patterns on the fabricated nickel mould. The remaining 30% might have a few scattered defects, caused by dust in the electroplating bath and slight unevenness of the e-beam resist coated on the wafer.

The gold nanoholes on the glass chip were kept in a highly consistent square shape as for the nanoholes written by e-beam in Fig. 2(b), which demonstrates the high fidelity of reproducing the originally designed nanopatterns. This is nontrivial in mass fabrication of metal nanostructures, because they cannot achieve such a high quality if a silicon mould is used. We investigated the process of fabricating a 4′′ silicon mould with a photolithography mask full of 3 μm × 3 μm microsized square holes and its subsequent nanoimprinting,[46] and ascertained that the micropatterns on the silicon mould were enlarged by 25% and became round due to the DRIE etching, and the polymer patterns after nanoimprinting

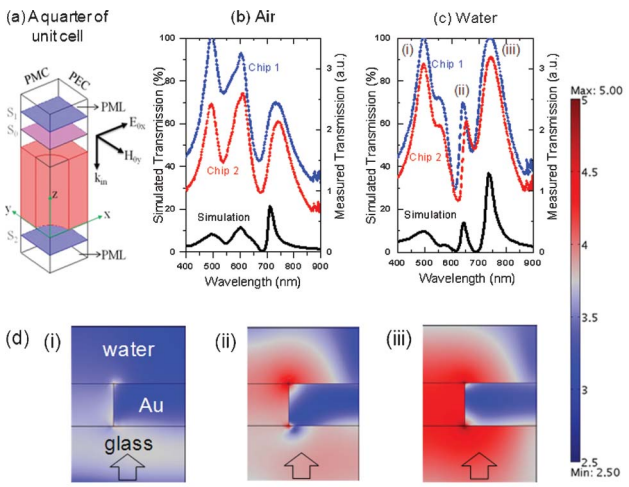

Fig. 5 (a) A quarter of the cell for simulation, and the simulated and measured transmission spectra of a gold nanohole array (b) in air and (c) in water, under normal incidence of light from the glass side. In (b) and (c), the black lines are the simulation results for the gold nanohole array with p = 400 nm, D = 150 nm, and T = 75 nm. The blue and red dotted lines represent the experimental results for two chips. (d) Cross-sectional view of the near field distributions (V m^{-1}) (in log scale) of the three plasmonic peaks identified in (c).

even became perfect circles, because each process step caused some loss of the pattern fidelity and fine detail.

To our best knowledge, nanoimprinting has been reported by several research groups to fabricate metal nanostructures,[34–42] but none of them has combined a nickel mould with UV nanoimprinting technology, which are the two important factors for us to achieve high fidelity and high yield in fabricating metal nanostructures. In our previous trials, the breakage of the wafers by using a silicon mould and thermal imprinting was high, while we did not experience any wafer breakage in the UV nanoimprinting with the nickel mould.

Time and cost saving is tremendous by using nanoimprinting to fabricate the gold nanohole array instead of e-beam lithography. For the nanohole array we designed, it took 40 h for the e-beam to write 25 2 mm × 2 mm areas on a 4′′ wafer, while nanoimprinting is completed within 20 min. The time saving is 120 times.

For the cost, with the same charge rate in the cleanroom at the Institute of Materials Research and Engineering (IMRE), the e-beam on the wafer (Fig. 2(a)) costs about 12.3 k USD, the nickel mould electroplating is 400 USD, and each wafer's nanoimprinting consumes 109 USD in materials and equipment usage. So the cost saving for nanoimprinting is 52, 71, and 101 times for the life-time of the nickel mould[24] to be 100, 200, and 1000 cycles. Our UV nanoimprinting uses a relatively low temperature and low pressure compared with thermal imprinting, thus the life-time of the nickel mould is expected to be much higher than thermal imprinting.

Above all, the complexity and high density of the patterns on the wafer will greatly increase the time and cost of the e-beam lithography, while they will not affect those of the nanoimprinting.

Optical spectra of the gold nanohole array

The dimensions of the gold nanostructures are designed for exciting the fluorescent dye Alexa 647. Our simulations suggested that when the chip is immersed in water, the gold nanohole array on glass with a pitch of p = 400 nm, diameter D = 150 nm, and thickness T between 50 and 100 nm will exhibit a plasmonic peak at the wavelength around 647 nm for Alexa 647 excitation.[45]

To examine the quality of our gold nanohole array compared with its original design, the transmission spectra of a pure gold nanohole array on glass (the sample presented in Fig. 4(c)) were measured in both air and water, and compared with our simulation results in Fig. 5.

The simulations in Fig. 5 were performed with COMSOL software (finite element method) based on total field calculations,[44] where a unit cell of a nanohole array was composed of a single nanohole embedded in a square box. Due to the geometrical symmetry, only a quarter of the unit cell was simulated with boundary conditions as shown in Fig. 5(a). The frequency-dependent dielectric function of gold was taken from the Palik handbook,[47] and the refractive indices for glass, air and water were taken as 1.52, 1.0, and 1.33, respectively. A normal incident plane wave (wavelength = 400–900 nm) was set up at the surface S_0 (where a boundary pair condition was applied). A linearly polarized plane wave travelling in the z direction was assumed to be x direction polarized. In order to mimic the entire nanohole array, the two boundaries perpendicular to the x-axis were set as perfect electric conductors (PEC), and the other two boundaries perpendicular to the y-axis were set as perfect magnetic conductors (PMC). The top (glass) and bottom (air/water) layers were defined as a perfect matched layer (PML) to absorb any scattered electromagnetic waves from the nanohole structure. As the incident wave struck the structure, the reflected power and transmitted power were calculated through the surface integration of the power flow over the surfaces S_1 and S_2, respectively. The absorbed power was computed through the volume integration of the resistive heating in the gold film (highlighted in red in Fig. 5(a)).

To ensure the accuracy of the simulations, the sum of the calculated reflected, transmitted and absorbed power was checked against the input incident power, and they were the same within <2% error.

Fig. 5(b) (black line) shows the transmission spectrum of the gold nanohole array with p = 400 nm, D = 150 nm, and T = 75 nm in air under normal light incidence from the bottom of the glass. The transmission spectrum for the same gold nanohole array immersed in water is shown in Fig. 5(c).

In real applications for detecting biological samples in water, we care more about the plasmonic modes in water as represented by the three peaks in Fig. 5(c), so the near field distributions of these peaks are shown in Fig. 5(d). Out of the three peaks, the second peak (ii) at the wavelength of 645 nm associates with strongly enhanced fields at the top rims of the gold nanoholes, which will be utilized for our dye excitation. When biological conjugated fluorescent dyes are bound close to the top rims of the nanoholes, the dyes will be strongly excited by this mode. For the first and third peaks, most of the optical energy is focused at the glass substrate side, which could not be utilized efficiently to excite the fluorescent dyes in water.

In addition, it is worth noting that the second and third peaks are tunable by varying the fabrication parameters of the nanohole array, that is, pitch, diameter and thickness.[44] This tunability can be easily achieved by our nanofabrication method. On the other hand, the first peak at around 500 nm is an intrinsic transmission peak associated with the gold film.[48]

In the same Fig. 5(b) and (c), we plotted our measured spectra of two fabricated chips in air and water (blue and red dotted lines). The predicted peaks in the simulations are all nicely reproduced. Above all, both chips clearly demonstrate a transmission peak at 640–650 nm in water, which is the plasmonic mode for our fluorescence enhancement and PSA measurements.

Fluorescence enhancement and PSA measurements

The gold nanohole array (p = 400 nm, square length = 140 nm, and T = 50 nm) on glass was used to excite the fluorescent dyes for prostate specific antigen (PSA) detection, as a proof-of-concept for the feasibility of using our fabricated gold nanohole arrays for biosensing. To check the sensitivity enhancement of the gold nanohole array, a 50 nm thick gold

film was coated on glass to repeat the same experiment as a control.

In our experiments, a 633 nm wavelength laser beam was illuminated on the gold nanohole array in the TE mode at a TIR angle of 71°. The results in Fig. 6(a) show that PSA detection based on the sandwich immunoassay on the gold nanohole array presents a linear intensity increment of 500 times, when the PSA concentration was increased from 100 pg ml^{-1} to 100 ng ml^{-1}. The LOD was determined to be 100 pg ml^{-1}, based on three times the standard deviation of the fluorescence response for blank samples. In the control experiment, the gold film achieved a LOD of only 1000 pg ml^{-1}. This LOD difference is because under the TE mode, no plasmonics are generated on the gold film, while the gold nanohole array still generates LSPR to enhance the fluorescence excitation.

To further investigate the plasmonic field distribution difference of the gold nanohole array and the gold film, simulation results are presented in Fig. 6(b)–(d).

To carry out an inclined-angle simulation, we modified some settings as compared to the previous normal-angle simulations. First, half of the unit cell simulated was changed to the one as shown in Fig. 6(b). Second, the two boundaries perpendicular to the incident electric-fields were still assumed to be perfect electric conductors (PEC), but the other two boundaries now were set at Floquet periodic boundary conditions where the incident angle could be defined. An inclined illumination angle of 71° in our nanohole array will generate the transmission spectrum shown in Fig. 6(c) (solid line). For comparison, the simulated transmission spectrum of a gold film is also shown (dashed line).

It is found that the nanohole array still shows the similar second peak with similar intensity in the same 640–650 nm range in water as in Fig. 5(c), regardless of the 71° incident angle and the reduced film thickness. The reduced film thickness tends to blue-shift the second peak and red-shift the third peak,[45] while the increased angle of incidence tends to red-shift the second peak and has no impact on the third peak (the figures are not shown here). Therefore, comparing the present transmission spectrum with the one in Fig. 5(c), the second peak does not shift but the third peak has a red-shift. Meanwhile, there is an intrinsic transmission in the low wavelength (~500 nm) region relevant to the gold film. Reducing the film thickness will increase this intrinsic transmission.

Most importantly, we plotted the near field distributions at 71° and 633 nm in Fig. 6(d). This confirms that there is a LSPR field distributed at the top rims of the gold nanoholes, while there is no obvious field intensity on the gold film surface. However, based on the transmission spectrum in Fig. 6(c), 10% of the light is transmitted to the top of the gold film surface, where the dyes are bound in the control experiment. So the dyes are still excited in the TE mode for the gold film, although the excitation is weak compared to the gold nanohole array.

Depending on the distance between the plasmonic hotspot and the dyes, the plasmonic field could either quench or enhance the fluorescent dye excitation. Further sensitivity increment is possible by optimizing the distance between the

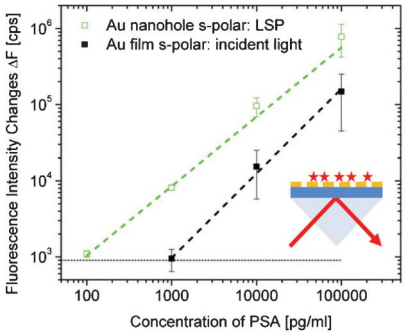

(a)

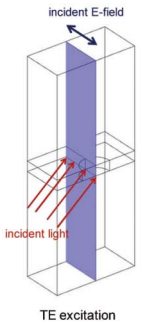

(b)

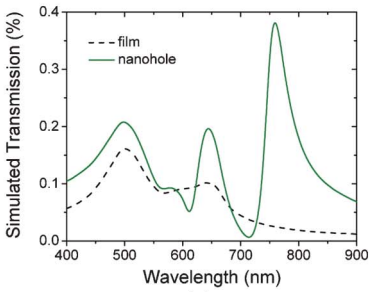

(c)

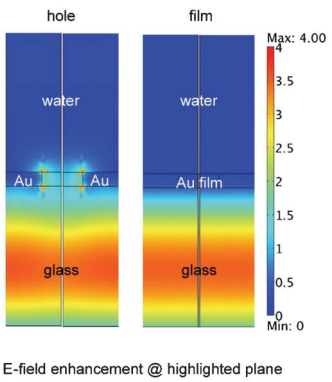

(d)

Fig. 6 (a) Fluorescence detection on a gold nanohole array (p = 400 nm, square length = 140 nm, T = 50 nm) and gold film (T = 50 nm) for a sandwich immunoassay of PSA at concentrations from 100 pg ml^{-1} to 100 ng ml^{-1}, where the 633 nm light is shed at 71° (the angle between the normal of the glass surface and the light beam) using TIR fluorescence spectroscopy in TE mode. (b) A half of a cell for plasmonic field simulation with angular incidence. (c) Transmission spectra and (d) plasmonic field distributions of the gold nanohole array and gold film on glass under the same conditions as in the experiments.

dyes and gold nanoholes. Although the antibody is approximately of size 14.2 nm × 8.5 nm × 4.0 nm,[49,50] with height close to the size of the plasmonic hot-spot, optimization of the distance between the dye and the nanoholes is possible, because at present the capturing antibodies are anchored on the gold surface, but they can also be anchored on the glass substrate only. Even the capturing antibodies are kept on the gold surface, because they are not standing upward (its thickness measured by dual polarization interferometry (DPI) is about 8.8 ± 1 nm[51]), still there is some room to optimize the distance between the dye and the gold nanoholes.

Conclusions

This paper has successfully developed a method to mass fabricate gold nanohole arrays for plasmonic based biosensors. Our method is to fabricate a nickel mould for wafer level UV nanoimprinting. By subsequently depositing a gold layer on the nanoimprinted photoresist and carrying out lift-off, pure gold nanohole arrays on a glass wafer are obtained with high yield. The measured transmission spectra of 75 nm thick gold nanohole arrays on glass match with our simulations. As a proof-of-concept, a 50 nm thick gold nanohole array on glass was used in a fluorescence excitation experiment, with TIR fluorescence spectroscopy at an angle of 71° and a wavelength of 633 nm. Through a c-Ab–PSA–d-Ab with Alexa647 assay, a detection limit of 100 pg ml^{-1} was achieved for PSA detection, which demonstrated a 10 times sensitivity enhancement compared with a gold film of the same thickness. The PSA detection sensitivity of the chip can be further improved by optimizing the distance between the dye and the plasmonic hotspots.

Acknowledgements

This research is supported by the Science and Engineering Research Council (SERC) of the Agency for Science, Technology and Research (A*STAR), with the project number of 102 152 0014. We are greatly indebted to the staff of the SERC nano fabrication, processing and characterisation (SnFPC) at the Institute of Materials Research and Engineering (IMRE) for their kind help and strong support. All of the fabrication process steps were conducted and characterized in SnFPC.

References

1 F. Yu, B. Persson, S. Lofås and W. Knoll, *Anal. Chem.*, 2004, **76**, 6765.
2 F. Yu, B. Persson, S. Lofås and W. Knoll, *J. Am. Chem. Soc.*, 2004, **126**, 8902.
3 J. R. Lakowicz, J. Malicka, E. Matveeva, I. Gryczynski and Z. Gryczynski, *Clin. Chem.*, 2005, **51**, 1914.
4 Y. Wang, A. Brunsen, U. Jonas, J. Dostálek and W. Knoll, *Anal. Chem.*, 2009, **81**, 9625.
5 M. J. Levene, J. Korlach, S. W. Turner, M. Foquet, H. G. Craighead and W. W. Webb, *Science*, 2003, **299**, 682.
6 A. G. Brolo, S. C. Kwok, M. G. Moffitt, R. Gordon, J. Riordon and K. L. Kavanagh, *J. Am. Chem. Soc.*, 2005, **127**, 14936.
7 A. G. Brolo, S. C. Kwok, M. D. Cooper, M. G. Moffitt, C.-W. Wang, R. Gordon, J. Riordon and K. L. Kavanagh, *J. Phys. Chem. B*, 2006, **110**, 8307.
8 J. Wenger, P.-F. Lenne, E. Popov, H. Rigneault, J. Dintinger and T. W. Ebbesen, *Opt. Express*, 2005, **13**, 7035.
9 H. Rigneault, J. Capoulade, J. Dintinger, J. Wenger, N. Bonod, E. Popov, T. W. Ebbesen and P.-F. Lenne, *Phys. Rev. Lett.*, 2005, **95**, 117401.
10 Y. Liu and S. Blair, *Opt. Lett.*, 2003, **28**, 507.
11 Y. Liu, J. Bishop, L. Williams, S. Blair and J. Herron, *Nanotechnology*, 2004, **15**, 1368.
12 P.-F. Guo, S. Wu, Q.-J. Ren, J. Lu, Z. Chen, S.-J. Xiao and Y.-Y. Zhu, *J. Phys. Chem. Lett.*, 2010, **1**, 315.
13 S. M. Tabakman, L. Lau, J. T. Robinson, J. Price, S. P. Sherlock, H. Wang, B. Zhang, Z. Chen, S. Tangsombatvisit, J. A. Jarrell, P. J. Utz and H. Dai, *Nat. Commun.*, 2011, **2**, 466.
14 S. Mayilo, M. A. Kloster, M. Wunderlich, A. Lutich, T. A. Klar, A. Nichtl, K. Kürzinger, F. D. Stefani and J. Feldmann, *Nano Lett.*, 2009, **9**, 4558.
15 R. Chhabra, J. Sharma1, H. Wang, S. Zou, S. Lin, H. Yan, S. Lindsay and Y. Liu, *Nanotechnology*, 2009, **20**, 485201.
16 Y. Chen, K. Munechika and D. S. Ginger, *Nano Lett.*, 2007, **7**, 690.
17 J. Zhao, X. Zhang, C. R. Yonzon, A. J. Haes and R. P. Van Duyne, *Nanomedicine*, 2006, **1**, 219.
18 H. Fredriksson, Y. Alaverdyan, A. Dmitriev, C. Langhammer, D. S. Sutherland, M. Zäch and B. Kasemo, *Adv. Mater.*, 2007, **19**, 4297.
19 G. Xiang, N. Zhang and X. Zhou, *Nanoscale Res. Lett.*, 2010, **5**, 818.
20 A. Dahlin, M. Zäch, T. Rindzevicius, M. Käll, D. S. Sutherland and F. Höök, *J. Am. Chem. Soc.*, 2005, **127**, 5043.
21 A. Kosiorek, W. Kandulski, H. Glaczynska and M. Giersig, *Small*, 2005, **1**, 439.
22 X. Zhou, K. Y. Liu, W. Knoll, C. Quan and N. Zhang, *Plasmonics*, 2010, **5**, 141.
23 O. Vazquez-Mena, T. Sannomiya, L. G. Villanueva, J. Vörös and J. Brugger, *ACS Nano*, 2011, **5**, 844.
24 *Handbook of Microlithography, Micromachining and Microfabrication*, ed. P. Rai-Choudhury, IET, 1997, p. 349.
25 S.-H. Kan, *US Pat.*, 20110046764 A1, 2009.
26 Y. Sawa, T. Tanaka, T. Kitadani, H. Ueno, K. Itoigawa, K. Yamashita, D. Noda and T. Hattori, *Microsyst. Technol.*, 2008, **14**, 1559.
27 Y. Sawa, K. Yamashita, T. Kitadani, D. Noda and T. Hattori, *Microsyst. Technol.*, 2010, **16**, 1369.
28 Z. H. Huang, B. C. Lim, T. T. Nguyen and Z. F. Wang, Mould inserts fabrication by photolithography and Ni electroforming processes, *SIMTech Technical Reports (STR_V12_N1_06_STG)*, 2011, **12**, 28.
29 L. J. Lee, M. J. Madou, K. W. Koelling, S. Daunert, S. Lai, C. G. Koh, Y.-J. Juang, Y. Lu and L. Yu, *Biomed. Microdevices*, 2001, **3**, 339.
30 Y. Hirai, S. Harada, H. Kikuta, Y. Tanaka, M. Okano, S. Isaka and M. Kobayasi, *J. Vac. Sci. Technol., B*, 2002, **20**, 2867.

31 T. G. Bifano, H. E. Fawcett and P. A. Bierden, *Precis. Eng.*, 1997, **20**, 53.
32 J. Arnold, U. Dasbach, W. Ehrfeld, K. Hesch and H. Löwe, *Appl. Surf. Sci.*, 1995, **86**, 251.
33 R. Turner, Y. Desta, K. Kelly, J. Zhang, E. Geiger, S. Cortez and C. Mancini, *J. Micromech. Microeng.*, 2003, **13**, 367.
34 N. C. Lindquist, P. Nagpal, K. M. McPeak, D. J. Norris and S.-H. Oh, *Rep. Prog. Phys.*, 2012, **75**, 036501.
35 J. M. Kontio, J. Simonen, J. Tommila and M. Pessa, *Microelectron. Eng.*, 2010, **87**, 1711.
36 S. Y. Lee, H. C. Jeon and S.-M. Yang, *J. Mater. Chem.*, 2012, **22**, 5900.
37 G. Barbillon, *Micromachines*, 2012, **3**, 21.
38 W. Wu, Z. Yu, S.-Y. Wang, R. S. Williams, Y. Liu, C. Sun, X. Zhang, E. Kim, Y. R. Shen and N. X. Fang, *Appl. Phys. Lett.*, 2007, **90**, 063107.
39 L. Jiao, H. Gao, G. Zhang, G. Xie, X. Zhou, Y. Zhang, Y. Zhang, B. Gao, G. Luo, Z. Wu, T. Zhu, J. Zhang, Z. Liu, S. Mu, H. Yang and C. Gu, *Nanotechnology*, 2005, **16**, 2779.
40 H. Schift, R. W. Jaszewski, C. David and J. Gobrecht, *Microelectron. Eng.*, 1999, **46**, 121.
41 S.-W. Ahn, K.-D. Lee, J.-S. Kim, S. H. Kim, S. H. Lee, J.-D. Park and P.-W. Yoon, *Microelectron. Eng.*, 2005, **78–79**, 314.
42 S. W. Lee, K. S. Lee, J. Ahn, J. J. Lee, M. G. Kim and Y. B. Shin, *ACS Nano*, 2011, **5**, 897.
43 Manual of the Alexa Fluor® 647 Protein Labeling Kit (A20173), http://tools.invitrogen.com/content/sfs/manuals/mp20173.pdf.
44 L. Wu, P. Bai and E. P. Li, *J. Opt. Soc. Am. B*, 2012, **29**, 521.
45 L. Wu, P. Bai, X. Zhou and E. P. Li, *IEEE Photonics J.*, 2012, **4**, 26.
46 T. I. Wong, H. Y. Ong, H. J. Lu, M. S. Tse, C. G. Quan, S. H. Ng and X. Zhou, *Microelectron. Eng.*, 2013, **104**, 64.
47 E. Palik, *Handbook of Optical Constants of Solids*, Elsevier, 1998.
48 S. Norrman, T. Andersson, C. G. Granqvist and O. Hunderi, *Phys. Rev. B*, 1978, **18**, 674.
49 E. W. Silverton, M. A. Navia and D. R. Davies, *Proc. Natl. Acad. Sci. U. S. A.*, 1977, **74**, 5140.
50 A. Ahluwalia, D. D. Rossi and A. Schirone, *Thin Solid Films*, 1992, **210–211**, 726.
51 H. Y. Song, X. Zhou, J. Hobley and X. D. Su, *Langmuir*, 2012, **28**, 997.